

Ab-initio Theory of Photoionization via Resonances

Adi Pick,^{1, a)} Petra Ruth Kaprálová-Žďánská,² and Nimrod Moiseyev^{1, b)}

¹⁾Faculty of Chemistry, Technion-Israel Institute of Technology, Haifa, Israel.

²⁾Department of Radiation and Chemical Physics, Institute of Physics, Academy of Sciences of the Czech Republic, Na Slovance 2, 182 21 Prague 8, Czech Republic

(Dated: 6 May 2019)

We present an *ab-initio* approach for computing the photoionization spectrum near autoionization resonances in multi-electron systems. While traditional (Hermitian) theories typically require computing the continuum states, which are difficult to obtain with high accuracy, our non-Hermitian approach requires only discrete bound and metastable states, which can be accurately computed with available quantum chemistry tools. We derive a simple formula for the absorption lineshape near Fano resonances, which relates the asymmetry of the spectral peaks to the phase of the complex transition dipole moment. Additionally, we present a formula for the ionization spectrum of laser-driven targets and relate the “Autler-Townes” splitting of spectral lines to the existence of exceptional points in the Hamiltonian. We apply our formulas to compute the autoionization spectrum of helium, but our theory is also applicable for non-trivial multi-electron atoms and molecules.

We present an *ab-initio* approach for computing the photoionization spectrum near autoionization (AI) resonances in multi-electron systems. Recent developments in attosecond-laser technology enable probing and controlling photoionization processes, and lead to a renewed interest in ionization and related phenomena, such as high-harmonic generation and strong-field electronic dynamics^{1–5}. These experimental capabilities call for *ab-initio* theories, which can relate the electronic structure of the sampled medium to the measured ionization spectrum. However, most existing theories require the calculation of the continuum states^{6,7} (above the ionization threshold), which are difficult to obtain with high accuracy with traditional methods^{8,9}. In this work, we use non-Hermitian quantum mechanics (NHQM)¹⁰ in order to avoid the need of computing continuum states. Our theory produces a simple formula for the “Fano asymmetry parameter” [Eq. (8)], which expresses the asymmetry of the peaks in the ionization spectrum near AI resonances¹¹, and a formula for the photoionization spectrum of laser-driven systems [Eq. (10)]. We relate the Autler-Townes¹² splitting of ionization spectral peaks to the existence of exceptional points¹³ (EPs)—special degenerate resonances where multiple AI states share the same energy and wavefunction. We demonstrate the predictions of our theory for helium using *ab-initio* electronic-structure data from Ref. 14,15. By using advanced non-Hermitian quantum-chemistry algorithms^{16,17}, our theory can also be applied for larger atoms and molecules.

In NHQM, the time-independent Schrödinger equation is solved with outgoing boundary conditions and the resulting energy spectrum is discrete, containing real-energy bound states and complex-energy metastable states¹⁰. This situation is very different from traditional Hermitian quantum mechanics (HQM), where metastable (autoionizing) states are described as real-energy bound states embedded in a continuum of free states¹¹. Moreover, in HQM, the transition dipole

moment is real, while in NHQM, it is generally complex. We show that the phase of the complex transition dipole moment has physical significance: it determines the asymmetry of the absorption peaks near AI states (see Fig. 1). Our derivation of the Fano asymmetry parameter is inspired by the recent work of Fukuta *et al.*¹⁸, which used a non-Hermitian approach to compute the Fano factor, although Ref. 18 introduced an artificial model for the continuum and did not relate the lineshape to the complex transition dipole moment.

As an application of our approach, we study the suppression and enhancement of photoionization in the presence of an external driving laser [Fig. 2]—two effects which are closely related to electromagnetically induced transparency (EIT)^{19–23} and absorption (EIA)^{24–26}. Laser-induced suppression of photoionization was first measured in magnesium^{27,28}, and later demonstrated in several other systems^{29,30}. These experiments were modeled using the Feshbach formalism^{28,31}, which requires the computation of the continuum states and can be avoided by our approach. Motivated by the huge impact of EIT in optics and atomic physics^{20–23}, we believe that the ability to accurately compute the analogous effects for AI states will open new routes for controlling and understanding photoionization and related phenomena (e.g., photoassociation and photodetachment).

We begin by reviewing the traditional theory of photoionization¹¹. In order to obtain the photoionization spectrum, one needs to compute the rate at which an absorbed photon excites an atom (or molecule) into an AI state. The transition rate induced by a linearly polarized electromagnetic field (with frequency ω , amplitude \mathcal{E} , and polarization axis \hat{x}) can be computed using Fermi’s golden rule³²

$$S(\omega) = \frac{|\mathcal{E}|^2}{\hbar} \sum_f^f |\langle \phi_i | x | \phi_f \rangle|^2 \delta(\hbar\omega - \varepsilon_f + \varepsilon_i). \quad (1)$$

Here, $\varepsilon_{i,f}$ and $|\phi_{i,f}\rangle$ are the initial- and final-state energies and wavefunctions respectively, while \sum_f^f denotes summation over bound and integration over continuum final states. The eigenfunctions and energies are obtained by diagonalizing the Hamiltonian (e.g., by using standard quantum-chemistry

^{a)}Also at Faculty of Electrical Engineering, Technion-Israel Institute of Technology, Haifa, Israel.; Electronic mail: pick.adi@gmail.com

^{b)}Also at Faculty of Physics, Technion-Israel Institute of Technology, Haifa, Israel.

tools³³). Since the continuum states have delocalized wavefunctions, it is challenging to compute them with the same level of accuracy as the bound states^{8,9}.

This difficulty can be circumvented by using the Green's function eigenstate-free method (developed in Refs. 32,34). In this approach, one first decomposes the Hamiltonian of the system into the “initial- and excited-state Hamiltonians,” defined as $\mathbb{H}_i \equiv \varepsilon_i |\phi_i\rangle\langle\phi_i|$ and $\mathbb{H}_{\text{exc}} \equiv \sum_f \varepsilon_f |\phi_f\rangle\langle\phi_f|$ respectively. The key idea of this approach is to realize that the summation in Eq. (1) can be avoided by exploiting the “excited-states' Green's function,” which is the impulse response of the operator \mathbb{H}_{exc} , defined as³⁵

$$\mathbb{G}_{\text{exc}}(\varepsilon) \equiv (\mathbb{H}_{\text{exc}} - \varepsilon)^{-1} = \sum_f \frac{|\phi_f\rangle\langle\phi_f|}{\langle\phi_f|\phi_f\rangle} \frac{1}{\varepsilon - \varepsilon_f}. \quad (2)$$

In the second equality, we employ the normal-mode expansion of the Green's function³⁶. Using a mathematical identity for the δ -function³⁷, one can rewrite Eq. (1) as

$$S(\omega) = \sum_f \langle\phi_i|x|\phi_f\rangle \left(\frac{1}{\hbar\pi} \text{Im} \lim_{s \rightarrow 0^+} \frac{|\mathcal{E}|^2}{\hbar\omega - is - \varepsilon_f + \varepsilon_i} \right) \langle\phi_f|x|\phi_i\rangle, \quad (3)$$

where the modes are normalized to one (i.e., $\langle\phi_f|\phi_f\rangle = 1$). Then, by substituting Eq. (2) into Eq. (3), one obtains

$$S(\omega) = \frac{|\mathcal{E}|^2}{\hbar\pi} \text{Im} \langle\phi_i|x \mathbb{G}_{\text{exc}} x|\phi_i\rangle, \quad (4)$$

where $\mathbb{G}_{\text{exc}}(\varepsilon)$ is evaluated at $\varepsilon = \hbar\omega + \varepsilon_i$.

Although Eq. (4) does not contain summation over continuum states [and is, therefore, more efficient than Eq. (1) in many cases], obtaining the excited-state Green's function of multi-electron systems requires significant computation power. However, the Green's function formulation naturally extends to NHQM, which offers a huge computational advantage. Under the conditions stated below, one can replace the Hermitian *normal-mode* expansion of G_{exc} [Eq. (2)] with the non-Hermitian *quasi-normal mode* expansion^{10,38}:

$$G_{\text{exc}}(\varepsilon) = \sum_f \frac{|\phi_f^R\rangle\langle\phi_f^L|}{\langle\phi_f^L|\phi_f^R\rangle} \frac{1}{\varepsilon - \varepsilon_f}. \quad (5)$$

Here, $|\phi_f^R\rangle$ and ε_f are the discrete eigenvectors and eigenvalues of the (non-Hermitian) time-independent Schrödinger equation—solved with outgoing boundary conditions—and $|\phi_f^L\rangle$ are the eigenvectors of the transposed Schrödinger equation. Round brackets denote the “unconjugated norm:” $(\phi|\psi) \equiv \int dx \phi \psi$ ¹⁰, which generalizes the traditional Dirac “conjugated norm,” $\langle\phi|\psi\rangle \equiv \int dx \phi^* \psi$ ³⁹ from HQM. Since the energy spectrum in NHQM is discrete, we replace \sum_f by Σ .

Equation 5 is valid assuming that (i) the Green's function is evaluated near the resonant energies (i.e., when $\varepsilon \approx \text{Re}[\varepsilon_f]$), (ii) the excited AI states, $\phi_f^R(x)$, are evaluated near the interaction region^{40,41} (i.e., not far from the atomic core, $|x| \approx a_0$, where a_0 is the Bohr radius), and (iii) when the energy spectrum does not contain EPs. Condition (i) is satisfied (in all

cases of interest) since we apply Eq. (5) only to study resonant absorption. Condition (ii) is fulfilled because the absorption formula [Eq. (4)] depends only on the overlap integral between extended AI states, $\phi_f^R(x)$, and localized bound states, $\phi_i^R(x)$. Although the eigenvectors of the non-Hermitian Hamiltonian, $\phi_f^R(x)$, are typically poor approximations for the “physical” metastable-state wavefunctions far from the interaction region (where they have diverging tails¹⁰), their unphysical values at large distances do not contribute to the absorption spectrum since the bound-state wavefunctions vanish at large distances. Last, when the energy spectrum contains EPs, Eq. (5) breaks down because the quasi-normal modes, $\phi_f^R(x)$, do not form a complete basis of the Hilbert space^{42–45}. At an EP, the “unconjugated norm” of the degenerate state, $(\phi_{\text{EP}}^L|\phi_{\text{EP}}^R)$, vanishes and the associated term in Eq. (5) blows up. One can obtain a corrected formula for G_{exc} at the EP by considering Eq. (5) *near the EP* and carefully taking the limit of approaching the EP. In this limit, the two terms in the sum that are associated with the nearly degenerate poles dominate the impulse response due to their infinitesimal denominators. However, one finds that two terms diverge with opposite signs, while their sum remains finite. This point was previously realized on pure mathematical grounds³⁸, and later explained in the context of electromagnetic modes^{42–45}. We sketch the derivation of the corrected formula for G_{exc} in the context of AI states in the supporting information (SI) appendix.

By substituting Eq. (5) into Eq. (4), we obtain the NHQM absorption spectrum formula:

$$S(\omega) = \frac{|\mathcal{E}|^2}{\hbar\pi} \text{Im} \sum_f \frac{(\phi_i^L|x|\phi_f^R)(\phi_f^L|x|\phi_i^R)}{(\phi_f^L|\phi_f^R)(\hbar\omega - \varepsilon_f + \varepsilon_i)}. \quad (6)$$

This formula applies to cases where the initial state is bound and, therefore, one can replace Dirac bracket states, $|\phi_i\rangle$ and $\langle\phi_i|$, with unconjugated bracket states $|\phi_i^R\rangle$ and $\langle\phi_i^L|$ (since the left eigenvector of a Hermitian Hamiltonian is equal to the conjugated right eigenvector of the same eigenvalue⁴⁶). However, when the initial state is metastable, one needs to keep the conjugated bracket for the initial state. Our derivation of Eq. (6) is similar in spirit to the recent work of Fukuta *et al.*¹⁸, which used NHQM to compute the absorption spectrum. However, the latter work introduced an artificial model for the continuum (which limits its generality) and did not relate the spectrum directly to the complex transition dipole moment.

Equation 6 applies both for autoionizing atoms and molecules. In either case, the AI rate depends on the complex transition moment between initial and final states of the system. While in atoms, ionizing transitions involve two different electronic states, in molecules (where the wavefunction depends both on electronic and nuclear coordinates), there are, generally speaking, two possibilities: (i) Either the initial and final electronic states are different but the nuclear rovibrational state is the same (as in penning ionization^{47–50} or interatomic Coulombic decay^{51–53}) or (ii) the initial and final electronic states are the same but the nuclear rovibrational state is different (as in dipole-bound anions⁵⁴ or intermolecular vibrational-energy transfer⁵⁵). In case (i) (which involves transitions between different electronic state), ionization can

occur provided that the energy of the excited electronic state exceeds the ground-state energy of the ion (i.e., the ionization threshold); under this condition, the excited state is degenerate with the continuum of free electronic states. Such processes are accurately described within the Born–Oppenheimer (BO) approximation, which amounts to assuming that the motion of atomic nuclei and electrons in a molecule can be separated⁵⁶. In case (ii) (which involves different nuclear rovibrational states), ionization happens due to non-adiabatic coupling terms (i.e., corrections beyond the BO approximation), which provide coupling between the electronic states of the molecule in different nuclear configuration. In order for AI to occur in such cases, the rovibrational energy must exceed the binding energy of the electron to the molecule. While the latter situation has been treated in Ref. 54, our new formula [Eq. (6)] applies to all cases. Note that Ref. 54 uses Hermitian scattering theory, while our approach uses NHQM, which makes the spectrum discrete and, therefore, produces a computationally efficient formula.

Our non-Hermitian formula [Eq. (6)] provides a simple formula for the “Fano asymmetry parameter,” which expresses the asymmetry of the peaks in the ionization spectrum near AI resonances¹¹. According to traditional absorption theory^{11,37}, the spectrum near an isolated resonance with frequency Ω and lifetime $1/\gamma$ can be written as

$$S_F(\omega) = S_0(\omega) \frac{(\omega - \Omega + \frac{\gamma}{2}q)^2}{(\omega - \Omega)^2 + (\frac{\gamma}{2})^2}, \quad (7)$$

where $S_0(\omega)$ is the background absorption due to continuum states and the remaining expression is the resonant peak. The parameter q determines the asymmetry of the resonant peak: in the limit of $q \rightarrow \infty$, the lineshape is Lorentzian, while the limit of $q \simeq 1$ produces an asymmetric lineshape. In traditional HQM, q is found by computing overlap integrals involving bound and continuum states^{11,37}. In our approach, however, the q factor depends on a single term in Eq. (6) (for which $\text{Re}[\varepsilon_f - \varepsilon_i] \approx \hbar\Omega$). By taking the ratio of the symmetric and anti-symmetric parts of that term (similar to Ref. 18), we obtain the compact expression

$$q = \left| \frac{\text{Re} \mu_{if}^2}{\text{Im} \mu_{if}^2} \right| \left[1 \pm \sqrt{1 + \left(\frac{\text{Im} \mu_{if}^2}{\text{Re} \mu_{if}^2} \right)^2} \right], \quad (8)$$

where we introduced a shorthand notation for the squared transition dipole moment, $\mu_{if}^2 \equiv (\phi_i^L | x | \phi_f^R) (\phi_f^L | x | \phi_i^R)$. The sign of q indicates whether the absorption peak is blue or red shifted, and is determined by the sign of $\text{Im} \mu_{if}^2$. More details on the derivation are given in the SI. Our formula for q generalizes an earlier result from Ref. 54, which analyzed molecular photodetachment. The formulas agree qualitatively in the limit of large q , which corresponds to nearly Lorentzian AI peaks. While in our case, this limit is attained for nearly real resonant energies, ε_f (which are associated with nearly real transition dipole moments, μ_{ij}), in Ref. 54, the ionization takes place due to non-adiabatic couplings and the limit of large q emerges when the BO approximation is nearly accurate (i.e., when the non-adiabatic couplings are small). A

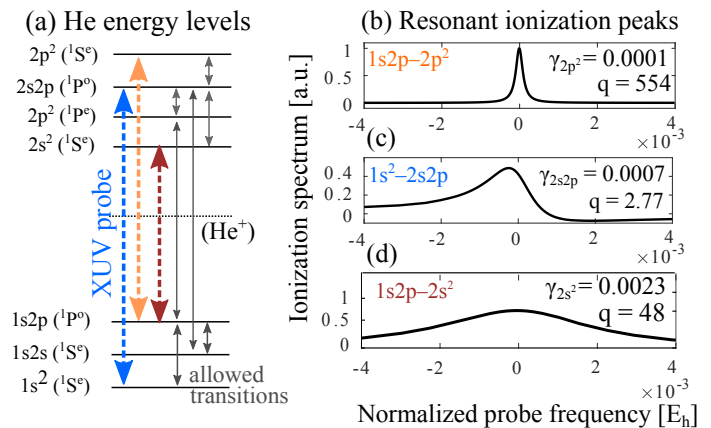


FIG. 1. (a) Orbitals of parahelium (labeled by spectroscopic notation⁵⁶), including three bound states and four autoionization resonances (above the ground-state energy of He^+). Thick dashed arrows mark the probed transitions, while narrow arrows mark additional dipole-allowed transitions. (b–d) Autoionization spectrum [evaluated using Eq. (6) using data from Ref. 15, summarized in Table S1 in the SI] near the three probed transitions from (a) and the associated q factors [evaluated using Eq. (8)]. The x -axis is the difference between the frequency of the field and the probed atomic transition. [e.g., in (b), “zero frequency” implies that the probe is resonant with the $1s2p \leftrightarrow 2p^2$ transition.]

quantitative comparison of the formulas and an application of our formula for molecular photodetachment will be addressed in future work.

As an example for application of Eq. (8), we compute the absorption lineshape near AI states in parahelium (i.e., helium atoms in which the spins of the two electrons are in the singlet state). The energy levels and dipole-allowed transitions are shown in Fig. 1(a). The states are labeled according to the approximate Hartree–Fock orbitals. All states below the ionization threshold are bound, while all double-excitation states are metastable AI states. We use data from Refs. 14,15 for the energy levels, lifetimes, and complex transition dipole moments (summarized in Table S1 in the SI). Figure 1(b–d) shows the ionization spectrum near three transitions in the XUV range, obtained by evaluating Eq. (6). The x -axis denotes the frequency offset between the field and the probed atomic transition. The plots demonstrate that our new formula for the Fano q factor [Eq. (8)] predicts the asymmetry of the lines, while the width of the peak is set by the imaginary part of the metastable-state energy.

Next, we turn to study photoautoionization in laser-driven atoms and molecules. Specifically, we consider cases where a “pump laser” couples two (or more) AI states and a “probe laser” drives transitions from the ground to the AI states. A time-periodic probed system (denoted below by H_0) has Floquet solutions the form⁵⁷:

$$\Psi_{\alpha,m}(x,t) = e^{-i\varepsilon_{\alpha,m}t/\hbar} \Phi_{\alpha,m}(x,t). \quad (9)$$

Here, $\Phi_{\alpha,m}$ and $\varepsilon_{\alpha,m}$ are the eigenvectors and eigenvalues of the Floquet Hamiltonian, $\mathcal{H} \equiv H_0 - i\hbar \frac{\partial}{\partial t}$. The eigenenergies are periodic in the frequency of the probe, ω_0 (i.e.,

$\varepsilon_{\alpha m} = \varepsilon_{\alpha,0} + m\hbar\omega_0$) and the eigenvectors obey $\Phi_{\alpha m}(t) = \Phi_{\alpha,0}(t)e^{i\omega_0 mt}$. The quantum number m is called the ‘‘Floquet channel.’’ In the SI, we use a generalized Fermi-Floquet golden rule⁵⁸ (which is valid for weak probe intensities) to derive a formula for the absorption spectrum of laser-driven systems. We obtain

$$S(\omega) = \frac{|\mathcal{E}|^2}{\hbar\pi} \text{Im} \sum_{f,m} \frac{((\Phi_{i,0}^L|x|\Phi_{f,m}^R))((\Phi_{f,m}^L|x|\Phi_{i,0}^R))}{\hbar\omega + m\hbar\omega_0 - \varepsilon_{f,0} + \varepsilon_{i,0}}. \quad (10)$$

Here $|\Phi_{i,0}\rangle$ and $|\Phi_{f,m}\rangle$ are the initial (bound) and final (metastable) Floquet states while $\varepsilon_{i,0}$ and $\varepsilon_{f,0}$ are the corresponding quasienergies in the zeroth Floquet channel. We use double brackets to denote spatial and temporal integration: $((\Phi|\Psi)) \equiv \frac{1}{T} \int_0^T dt' \int_{-\infty}^{\infty} dx \Phi(t',x)\Psi(t',x)$. In order to evaluate Eq. (10), it is convenient to expand the Floquet states, $|\Phi_{f,m}\rangle$, in the basis of eigenvectors of the field-free Hamiltonian. In the SI, we review this standard procedure^{59,60} and present an explicit expression for the spectrum in terms of field-free eigenstates [Eq. (C22)].

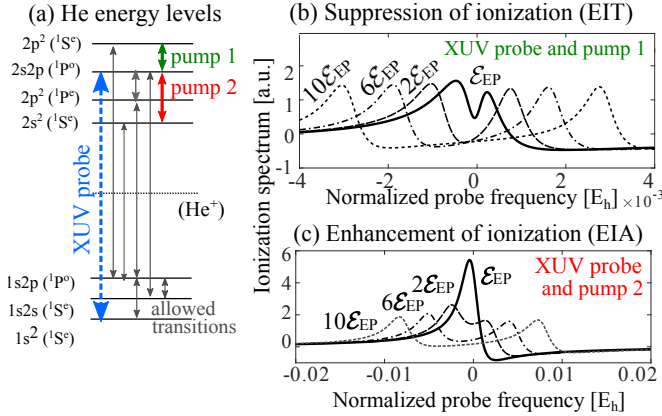


FIG. 2. (a) Orbitals of parahelium (as in Fig. 1). Thick dashed (solid) arrows mark the probed (pumped) transitions, while narrow arrows mark other allowed transitions. (b) Pump 1 couples the probed AI state [$2s2p(1P^o)$] to the state $2p^2(1S^e)$, whose lifetime is longer than $2s2p$. The pump produces a dip in the ionization spectrum when the probe is resonant with the probed transition, similar to EIT. (The x -axis is the probe’s detuning from resonance, as in Fig. 1.) Four pump amplitudes are shown: $\mathcal{E}/\mathcal{E}_{EP} = 1, 2, 6, 10$, while the pump intensity is ω_2^{EP} (see text). Helium parameters are summarized in Table S1. (c) Pump 2 couples the probed AI state to the state $2s^2(1S^e)$, whose lifetime is shorter than $2s2p$. The resulting ionization spectrum shows enhancement of ionization on resonance (similar to EIA).

Next, we apply Eq. (10) to compute the autoionization spectrum of laser-driven parahelium. As shown in Fig. 2(a), we consider an XUV probe, which drives the transition between the ground state [$1s^2(1S)$] and the AI state $2s2p(1P)$ and a strong NIR pump, which resonantly couples two AI states. We consider two cases: (i) The pump couples $2s2p(1P)$ and $2p^2(1S)$ (green arrow) and (ii) The pump couples $2s2p(1P)$ and $2s^2(1S)$ and (red arrow). The difference between the two cases is that in the former, the probe couples the ground state to the broader AI state (out of the two coupled AI states),

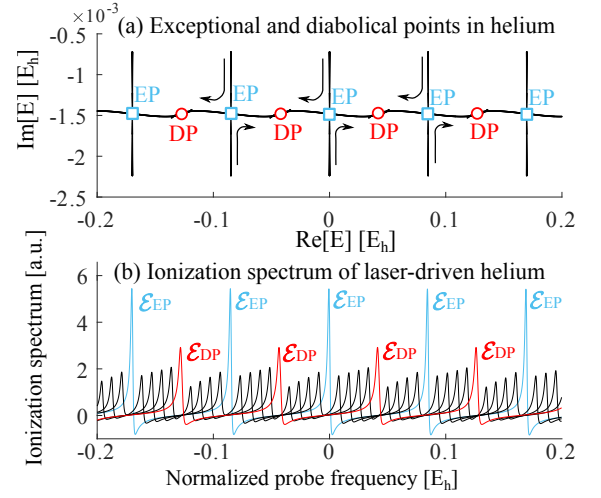


FIG. 3. (a) Trajectories of eigenvalues of the Floquet Hamiltonian [Eqs. (C6-C7)] upon varying the pump amplitude across the EP value while fixing the pump frequency at ω_2^{EP} (see text). Helium parameters are summarized in Table S1. Pairs of eigenvalues merge at exceptional and diabolical points (EPs and DPs), marked by cyan triangles and red circles respectively. (b) Relative absorption as a function of probe detuning for six pump amplitudes: $\mathcal{E}_0/\mathcal{E}_{EP} = 1, 11, 22, 33, 44, 55$. The peak absorption at EPs (cyan solid) is twice larger than DPs (red dashed). The x -axis denotes the frequency offset between the field and the probed atomic transition.

while in the latter, the probe couples the ground state to the narrower AI state. It turns out that these two situations lead to drastically different ionization spectra. In the former case [shown in Fig. 2(b)], the effect of the pump is to suppress the ionization when the probe-photon energy is resonant with the atomic transition. The narrow dip in the autoionization spectrum is similar in spirit to the transparency window in EIT. As shown in the early work of Ref. 27, the suppression occurs due to coherent trapping of the atomic population in the ground state. In contrast, in the latter case [shown in Fig. 2(c)], the ionization lineshape is Lorentzian for weak pump amplitudes [similar to electromagnetically induced absorption (EIA)]. As the pump exceeds a critical value (denoted by $\mathcal{E}_0 = \mathcal{E}_{EP}$), the peak splits into two non-overlapping dressed-state peaks. At the splitting point, the Hamiltonian has an EP, as discussed below. Panels (b–c) show the splitting of the ionization peaks upon increasing the pump amplitude beyond the critical point (we show four pump values $\mathcal{E}_0/\mathcal{E}_{EP} = 1, 2, 6, 10$). Our *ab-initio* calculation takes into account all the dipole-allowed transitions in parahelium, although the atomic population predominantly occupies only three states in all cases under study.

When the pump amplitude significantly exceeds \mathcal{E}_{EP} (at $\mathcal{E} \approx 70\mathcal{E}_{EP}$), pairs of resonances merge again at ordinary degeneracies, called diabolical points (DPs). The trajectories of the complex eigenvalues of the Floquet Hamiltonian [see SI, Eqs. (C6-C7)] are shown in Fig. 3(a). Panel (b) shows the absorption spectrum at varying pump intensities for the case where the pump couples $2s^2(1S)$ and $2s2p(1P)$ [case (ii) above]. The plot demonstrates that the peak of the ionization spectrum near the EPs is significantly larger than near the DPs

(i.e., four-fold instead of two-fold), although the imaginary parts of the degenerate eigenvalues are approximately equal. This demonstrates the increased density of states at EPs (similar to the effect shown in spontaneous emission near EPs in Maxwell's equations⁴⁵).

In order to see that the point at which the spectral peaks split is an EP, we introduce a simplified model, where we keep only three electronic states (i.e., we keep only the ground state and a pair of AI state) and employ the rotating wave approximation⁶¹ (RWA) to eliminate rapidly rotating terms due to the pump and the probe. By using the RWA, a three-level system can be described by the stationary effective Hamiltonian^{61,62}:

$$\mathbb{H} = \left(\begin{array}{c|cc} E_g + \hbar\omega_1 & -\frac{\mu_1 \mathcal{E}_1}{2} & 0 \\ \hline -\frac{\mu_1 \mathcal{E}_1}{2} & E_1 - i\gamma_1 & -\frac{\mu_2 \mathcal{E}_2}{2} \\ \hline 0 & -\frac{\mu_2 \mathcal{E}_2}{2} & E_2 - i\gamma_2 - \hbar\omega_2 \end{array} \right) \quad (11)$$

Here, E_g is the real ground-state energy, $E_{1,2}$ and $\gamma_{1,2}^{-1}$ are the excited-state energies and lifetimes and $\mu_{1,2}$ are the complex transition dipole moments of the allowed transitions. $\omega_{1,2}$ and $\mathcal{E}_{1,2}$ are the frequencies and amplitudes of the probe and pump fields respectively. The solid lines in Eq. (11) mark the excited-state Hamiltonian, \mathbb{H}_{exc} (introduced in the introduction), whose complex eigenvalues (ε_{\pm}) and eigenvectors (ϕ_{\pm}) coalesce at an EP when the pump frequency and amplitude are⁶²

$$\hbar\omega_2^{\text{EP}} \equiv E_1 - E_2 + \frac{\gamma_2 - \gamma_1}{2} \frac{\text{Im} \mu_2}{\text{Re} \mu_2}, \quad \mathcal{E}_2^{\text{EP}} \equiv \pm \frac{\gamma_1 - \gamma_2}{2 \text{Re} \mu_2}, \quad (12)$$

More details are given in the SI. When the pump intensity is fixed at ω_2^{EP} and its amplitude exceeds the critical value of $\mathcal{E}_2^{\text{EP}}$, the ionization peak splits into two since the dressed-state energies, $\text{Re}[\varepsilon_{\pm}]$, become non degenerate. Similar to our conclusion here, it was also noted in Ref. 27 that the splitting of spectral lines occurs when “the dipole coupling is strong enough to compete with the autoionizing width.” However, our non-Hermitian approach enables to identify this point as an EP and, therefore, opens the possibility of exploring EP-related effects near the splitting point.

To summarize, we presented an *ab-initio* theory of resonant photoionization. Our derivation produced accurate formulas for the ionization spectrum, which are of current interest due to recent developments in experimental capabilities for probing and controlling ionization processes. By using NHQM, our theory avoids the need of computing the continuum states, which are required by the traditional Feshbach formalism. As an application of our theory, we derive a simple expression for the Fano asymmetry factor. Moreover, we study autoionization in laser driven systems and show that the splitting of spectral lines occurs at EPs. This work opens several directions for future study. For example, the non-trivial topological phase associated with the EP⁶³ can be used to transition between nearly degenerate states in a topologically protected manner⁶⁴, and may have practical applications for controlling the ionization spectrum. Another example for an EP-related effect is the enhanced density of states at the EP. Previous work on spontaneous

emission^{45,65} shows that the emission rate can be significantly enhanced by placing the emitter near pumped resonators with EPs (i.e., using systems that have optical gain). Along similar lines, one can expect enhanced autoionization rates in systems with gain of atomic population in particular AI states. Such a situation can be engineered, for example, (e.g., in systems with cycling transitions⁶⁶). Finally, the present work treated broadening of absorption lines due to autoionization, but can be extended to include other line-broadening mechanism (such as vibrational and Doppler broadening) by combining NHQM with a Lindbladian formulation.

ACKNOWLEDGMENTS

AP is partially supported by an Aly Kaufman Fellowship at the Technion. NM acknowledges the financial support of I-Core: The Israeli Excellence Center “Circle of Light,” and of the Israel Science Foundation Grant No. 1530/15. PRK acknowledges the financial support by the Czech Ministry of Education, Youth and Sports, program INTER-EXCELLENCE (Grant LTT17015). Finally, the authors thank Christiana Koch, Michael Rosenbluh, Hossein Sadeghpour, Uri Peskin, Saar Rahav, Gad Bahir, and Ofer Neufeld for insightful discussions.

SUPPLEMENTARY INFORMATION

I. GREEN'S FUNCTION NEAR EPS

Near an EP, the non-Hermitian normal-mode expansion formula for the Green's function [Eq. (5)] breaks down. In this appendix, we review the derivation of the modified expansion formula which is valid at the EP, following⁴⁵. Consider the parameter-dependent Hamiltonian:

$$H(\xi) = H_0 + \xi V \quad (\text{A1})$$

where H_0 is defective (i.e., the point $\xi = 0$ is an EP in parameter space). At the EP, the set of eigenvectors is no longer a complete basis of the Hilbert space. To remedy this problem, we introduce additional Jordan vectors. At a second-order EP, the Jordan vector $|j_{\text{EP}}\rangle$ is defined via the chain relations

$$\begin{aligned} H_0|\phi_{\text{EP}}\rangle &= \varepsilon_{\text{EP}}|\phi_{\text{EP}}\rangle, \\ H_0|j_{\text{EP}}\rangle &= \varepsilon_{\text{EP}}|j_{\text{EP}}\rangle + |\phi_{\text{EP}}\rangle. \end{aligned} \quad (\text{A2})$$

where ε_{EP} and ϕ_{EP} are the degenerate eigenvalue and eigenvector and the self-orthogonality condition [$(\phi_{\text{EP}}|\phi_{\text{EP}}) = 0$] is automatically satisfied. Following⁶⁷, we choose the normalization conditions $(\phi_{\text{EP}}|j_{\text{EP}}) = \varepsilon_{\text{EP}}^{-1}$ and $(j_{\text{EP}}|j_{\text{EP}}) = 0$. Near the EP at $\xi = 0$, the Hamiltonian $H(\xi)$ has a pair of nearly degenerate eigenenergies and nearly parallel eigenvectors. They can be approximated by a Puiseux series, which contains fractional powers in the small parameter ξ ⁶⁷:

$$\begin{aligned} \varepsilon_{\pm} &= \varepsilon_{\text{EP}} + \sqrt{\xi} \mathcal{V} + \mathcal{O}(\xi) \\ |\phi_{\pm}\rangle &= |\phi_{\text{EP}}\rangle + \sqrt{\xi} \mathcal{V} |j_{\text{EP}}\rangle + \mathcal{O}(\xi) \end{aligned} \quad (\text{A3})$$

where

$$\mathcal{V} = \sqrt{\frac{(j_{\text{EP}}|V|\phi_{\text{EP}})}{(j_{\text{EP}}|\phi_{\text{EP}})}}. \quad (\text{A4})$$

Now, let us return to the modal expansion formula of G [Eq. (5)], which is valid for $\xi \neq 0$. Near the EP, the expansion is dominated by the two terms of the coalescing resonances. Keeping just these two terms in the sum, we can write

$$G(\varepsilon) = \frac{1}{\varepsilon - \varepsilon_+} \frac{|\phi_+\rangle(\phi_+|)}{(\phi_+|\phi_+)} + \frac{1}{\varepsilon - \varepsilon_-} \frac{|\phi_-\rangle(\phi_-|)}{(\phi_-|\phi_-)} \quad (\text{A5})$$

Next, we substitute the approximate expressions for $|\phi_{\pm}\rangle$ and ε_{\pm} [Eq. (A3)] into Eq. (A5) and, by carefully taking the limit of $\xi \rightarrow 0$, we obtain⁴⁵

$$\begin{aligned} G(\varepsilon) &= \frac{1}{(\varepsilon - \varepsilon_{\text{EP}})^2} \frac{|\phi_{\text{EP}}\rangle(\phi_{\text{EP}}|}{(\phi_{\text{EP}}|j_{\text{EP}})} + \\ &\frac{1}{\varepsilon - \varepsilon_{\text{EP}}} \left(\frac{|\phi_{\text{EP}}\rangle(j_{\text{EP}}|}{(\phi_{\text{EP}}|j_{\text{EP}})} + \frac{|j_{\text{EP}}\rangle(\phi_{\text{EP}}|)}{(\phi_{\text{EP}}|j_{\text{EP}})} \right) \end{aligned} \quad (\text{A6})$$

The double pole at ε_{EP} dominates the absorption spectrum near the EP.

II. NON-HERMITIAN FANO FACTOR

In this appendix, we derive Eq. (8) from the main text. The formula is obtained by comparing the ratio of the symmetric and antisymmetric parts of our new spectral formula [Eq. (6)] and the Fano lineshape near a single resonance [Eq. (7)]. First, let us introduce the dimensionless detuning parameter $x = \frac{\omega - \Omega}{\gamma/2}$ and rewrite Eq. (7) as

$$S_F = 1 + \frac{2xq}{x^2 + 1} + \frac{q^2 - 1}{x^2 + 1} \quad (\text{B1})$$

Next, let us define the symmetric and antisymmetric parts of our absorption formula as

$$\begin{aligned} S_{\text{symm}} &= \frac{|\mathcal{E}|^2}{\hbar\pi} \frac{\text{Re} \mu_{if}^2 \text{Im} \varepsilon_f}{(\omega - \text{Re} \varepsilon_f)^2 + (\text{Im} \varepsilon_f)^2}, \\ S_{\text{asymm}} &= \frac{|\mathcal{E}|^2}{\hbar\pi} \frac{\text{Im} \mu_{if}^2 (\text{Re} \varepsilon_f - \omega)}{(\omega - \text{Re} \varepsilon_f)^2 + (\text{Im} \varepsilon_f)^2}, \end{aligned} \quad (\text{B2})$$

where introduced the shorthand notation $\mu_{if}^2 = (\phi_i^L|x|\phi_f^R)(\phi_f^L|x|\phi_i^R)$. By comparing Eq. (B1) and Eq. (B2) we find that

$$\frac{2q}{q^2 - 1} = \frac{\text{Im} \mu_{if}^2}{\text{Re} \mu_{if}^2}. \quad (\text{B3})$$

The solution of Eq. (B3) yields the Fano asymmetry factor [Eq. (8)]. The sign of q is determined by the sign of $\text{Im} \mu_{if}^2$. When $q > 0$, the absorption is stronger at frequencies higher than the resonance frequency and weaker below the resonance. When $q < 0$, the contrary is true.

III. ABSORPTION IN LASER-DRIVEN SYSTEMS

A. The Floquet Hamiltonian

In this section, we explain how to construct the Floquet Hamiltonian and find its eigenvalues and eigenvectors, which appear in Eq. (10) in the main text. We wish to solve the Floquet eigenvalue problem

$$\mathcal{H}\Phi_\alpha = \varepsilon_\alpha \Phi_\alpha, \quad (\text{C1})$$

where

$$\mathcal{H} \equiv H_0 + \mathcal{E}x \cos \omega_0 t - i\hbar \partial_t. \quad (\text{C2})$$

In order to solve Eq. (C1) numerically, we introduce M temporal Fourier basis states, $f_m(t) = e^{i\omega m t}$, and N spatial field-free states, $\phi_\mu^{\text{FF}}(x)$. Invoking the completeness relation,

$$\mathbb{1} = \sum_{m=1}^M |f_m(t)\rangle \langle f_m(t)| \otimes \sum_{\mu=1}^N |\phi_\mu^{\text{R,FF}}(x)\rangle \langle \phi_\mu^{\text{L,FF}}(x)|, \quad (\text{C3})$$

we can rewrite Eq. (C1) in matrix form:

$$\sum_{m,\nu} (n, \nu | \mathcal{H} | m, \mu) (m, \mu | \Phi_\alpha) = \varepsilon_\alpha (n, \nu | \Phi_\alpha) \quad (\text{C4})$$

or in shorthand notation:

$$\overline{\overline{\mathcal{H}}}\overline{\Phi}_\alpha = \varepsilon_\alpha \overline{\Phi}_\alpha, \quad (\text{C5})$$

where $\overline{\overline{\mathcal{H}}}$ is block diagonal, with block size $M \times M$. The diagonal blocks are associated with the first and last terms in Eq. (C2)

$$\overline{\overline{\mathcal{H}}}_{\mu n, \nu n} = (\varepsilon_\mu^{\text{FF}} + n\hbar\omega_0)\delta_{\mu, \nu} \quad (\text{C6})$$

and the off-diagonal elements come from the second term:

$$\overline{\overline{\mathcal{H}}}_{\mu n, \nu n \pm 1} = \frac{\mathcal{E}}{2} (\phi_\mu^{\text{L,FF}} |x| \phi_\nu^{\text{R,FF}}) \quad (\text{C7})$$

B. Fermi-Floquet absorption formula

In this appendix, we complete the derivation of Eq. (10) from the main text. Our derivation is inspired by Ref.⁵⁸, which analyzes scattering from a time-periodic potential. Consider an atom or molecule, which interacts with a laser at frequency ω_0 . The system is described by the Hamiltonian H_0 , whose eigenstates are Floquet states, as explained in the main text. The propagator of H_0 is defined via

$$i\hbar\partial_t U_0(t_0, t) = H_0(t)U_0(t_0, t). \quad (\text{C8})$$

We also introduce a weak laser, hereafter called ‘‘the probe,’’ with frequency ω . The total Hamiltonian is

$$H = H_0 + V, \quad (\text{C9})$$

where the interaction term is $V = \mathcal{E}xe^{i\omega t}$. In order to derive Fermi-Floquet golden rule, we move to the interaction picture, where states and operators are defined as

$$\begin{aligned} |\Psi^I(t)\rangle &= U_0(t, t_0)|\Psi(t)\rangle \\ \mathcal{O}^I(t) &= U_0(t, t_0)\mathcal{O}U_0(t_0, t). \end{aligned} \quad (\text{C10})$$

Note that the total propagator, defined as

$$i\hbar\partial_t U(t_0, t) = H(t)U(t_0, t), \quad (\text{C11})$$

can be written as a product of the unperturbed and interaction-picture propagators:

$$U(t_0, t) = U_0(t_0, t)U^I(t_0, t). \quad (\text{C12})$$

The last statement can be verified by substituting Eq. (C12) into Eq. (C11), applying the chain rule to compute $\partial_t U(t, t_0)$, and using Eq. (C8) and $V^I = U_0(t, t_0)VU_0(t_0, t)$.

Next, we compute the transition amplitude between Floquet states $|\Psi_f(t)\rangle$ and $|\Psi_i(t)\rangle$, where i and f are super-indexes which denote the field-free state and the channel. The transition amplitude is

$$\begin{aligned} A(i \rightarrow f, t) &= \langle \Psi_f(t) | U(0, t) | \Psi_i(0) \rangle = \\ &= \langle \Psi_f(t) | U_0(0, t) U^I(0, t) | \Psi_i(0) \rangle = \\ &= \langle \Psi_f(0) | U^I(0, t) | \Psi_i(0) \rangle \end{aligned} \quad (\text{C13})$$

We use a Dyson series to express the interaction-picture propagator, U^I , in terms of V^I . Keeping terms up to the first order in V^I , one obtains:

$$U^I(t_0, t) = \mathbb{1} - \frac{i}{\hbar} \int_{t_0}^t dt' V^I(t') + \mathcal{O}(V^2). \quad (\text{C14})$$

Substituting Eq. (C14) into Eq. (C13), one obtains

$$\begin{aligned} A(i \rightarrow f, t) &= \frac{-i}{\hbar} \int_0^t dt' \langle \Psi_f(0) | V^I(0, t') | \Psi_i(0) \rangle = \\ &= \frac{-i}{\hbar} \int_0^t dt' \langle \Psi_f(0) | U_0(t', 0) V U_0(0, t') | \Psi_i(0) \rangle = \\ &= \frac{-i}{\hbar} \int_0^t dt' e^{-i(\varepsilon_i - \varepsilon_f)t'/\hbar} \langle \Phi_f(t') | V | \Phi_i(t') \rangle. \end{aligned} \quad (\text{C15})$$

Since the Floquet states $\Phi_\alpha(x, t)$ are periodic in time, one can decompose them into Fourier components

$$\Phi_\alpha(x, t) = \sum_n e^{i\omega_0 n t} \tilde{\Phi}_{\alpha, n}(x) \quad (\text{C16})$$

where the Fourier components of the wavefunction are $\tilde{\Phi}_{\alpha, n}(x) \equiv \frac{1}{\sqrt{2\pi}} \int_{-\infty}^{\infty} dt \Phi_\alpha(x, t) e^{-i\omega_0 n t}$. Using this expansion, the transition amplitude becomes

$$\begin{aligned} A(i \rightarrow f, t) &= \\ &= \sum_{mn} \frac{-i\mathcal{E}}{\hbar} \int_0^t dt' e^{-i(\varepsilon_i - \varepsilon_f - (n-m)\hbar\omega_0 - \hbar\omega)t'/\hbar} \langle \tilde{\Phi}_{f, n} | x | \tilde{\Phi}_{i, m} \rangle = \\ &= \mathcal{E} \sum_{mn} \frac{e^{-i(\varepsilon_i - \varepsilon_f - m\hbar\omega_0 - \hbar\omega)t/\hbar} - 1}{\varepsilon_i - \varepsilon_f - m\hbar\omega_0 - \hbar\omega} \langle \tilde{\Phi}_{f, m+n} | x | \tilde{\Phi}_{i, m} \rangle. \end{aligned} \quad (\text{C17})$$

The absorption spectrum can be found by taking the time average of the transition probability:

$$S(\omega) \equiv \frac{1}{T} \int_0^T dt \frac{d}{dt} |A_{if}|^2 = 2\text{Re} \left[\frac{1}{T} \int_0^T dt A^* \frac{dA}{dt} \right], \quad (\text{C18})$$

where T is a large integer multiple of the oscillation period $\frac{2\pi}{\omega_0}$. Substituting Eq. (C17) into Eq. (C18) and neglecting rapidly oscillating terms, we obtain

$$\frac{1}{T} \int_0^T dt A^* \frac{dA}{dt} = \frac{-i|\mathcal{E}|^2}{\hbar} \sum_{mnl} \frac{\langle \tilde{\Phi}_{f, m+n} | x | \tilde{\Phi}_{i, m} \rangle \langle \tilde{\Phi}_{i, m} | x | \tilde{\Phi}_{f, m+l} \rangle}{(\varepsilon_i - \varepsilon_f - m\hbar\omega_0 - \hbar\omega)} \quad (\text{C19})$$

Finally, we take the real part of Eq. (C19) and arrive at

$$S(\omega) = \frac{|\mathcal{E}|^2}{\hbar} \text{Im} \left[\sum_{mnl} \frac{\langle \tilde{\Phi}_{f, m+n}^L | x | \tilde{\Phi}_{i, m}^R \rangle \langle \tilde{\Phi}_{i, l}^L | x | \tilde{\Phi}_{f, l+m}^R \rangle}{\varepsilon_i - \varepsilon_f - m\hbar\omega_0 - \hbar\omega} \right] \quad (\text{C20})$$

The last formula can be rewritten compactly as Eq. (10) in the main text.

C. Autoionization spectral formula in the field-free basis

In order to evaluate our new formula for the absorption spectrum [Eq. (C20) or equivalently Eq. (10) from the main

text], we need to know the Fourier transforms of Floquet states. However, standard quantum chemistry methods solve the field-free problem, and we would like to use the field-free basis states and avoid the formidable task of solving the Floquet eigenvalue problem for a multielectron atom or molecule. To this end, we expand the Fourier transforms of the Floquet states in the basis of field-free states.

$$|\tilde{\phi}_{\alpha,n}\rangle = \sum_{\mu} (\phi_{\mu}^{\text{FF}} | \tilde{\phi}_{\alpha,n} \rangle | \phi_{\mu}^{\text{FF}}) \quad (\text{C21})$$

Substituting Eq. (C21) into Eq. (C20), we obtain

$$S(\omega) = \frac{|\mathcal{E}|^2}{\hbar} \text{Im} \left[\sum_{\substack{mn\ell \\ \mu\nu\sigma\tau}} (\tilde{\phi}_{i,\ell}^L | \phi_{\tau}^{\text{FF}}) (\phi_{\tau}^{\text{FF}} | x | \phi_{\sigma}^{\text{FF}}) \right. \\ \left. \frac{(\phi_{\sigma}^{\text{FF}} | \tilde{\phi}_{f,\ell+m}^R) (\tilde{\phi}_{f,n+m}^L | \phi_{\mu}^{\text{FF}})}{\varepsilon_i - \varepsilon_f - m\hbar\omega_0 - \hbar\omega} (\phi_{\mu}^{\text{FF}} | x | \phi_{\nu}^{\text{FF}}) (\phi_{\nu}^{\text{FF}} | \tilde{\phi}_{i,n}^R) \right] \quad (\text{C22})$$

The transition dipole moments between field-free states, $(\phi_{\tau}^{\text{FF}} | x | \phi_{\sigma}^{\text{FF}})$, are obtained directly from available quantum chemistry codes. By construction, the expansion coefficients, $(\phi_{\mu}^{\text{FF}} | \tilde{\phi}_{\alpha,n}^R)$, are the components of the eigenvectors of the Floquet matrix:

$$(\phi_{\mu}^{\text{L,FF}} | \tilde{\phi}_{\alpha,m}^R) = (m, \mu | \Phi_{\alpha}^R). \quad (\text{C23})$$

The eigenvectors of the Floquet Hamiltonian, $(m, \mu | \Phi_{\alpha}^R)$, are defined in Eq. (C4).

D. EPs in the Floquet Hamiltonian

To get an initial guess for the location of the EP, it is convenient project the full Hamiltonian onto the field-free excited states ψ_2 and ψ_3 and use the rotating wave approximation, which gives the 2×2 Hamiltonian

$$H_{\text{exc}} = \begin{pmatrix} E_2 & -\frac{\mu_{23}\mathcal{E}}{2} \\ -\frac{\mu_{32}\mathcal{E}}{2} & E_3 - \hbar\omega_0 \end{pmatrix}. \quad (\text{C24})$$

Subtracting E_2 from the diagonal and introducing the definitions $\delta \equiv \text{Re}[E_3 - E_2 - \hbar\omega_0]$ and $\Gamma \equiv -2\text{Im}[E_3 - E_2]$, we obtain

$$H_{\text{exc}} = \begin{pmatrix} 0 & -\frac{\mu_{23}\mathcal{E}}{2} \\ -\frac{\mu_{23}\mathcal{E}}{2} & \delta - i\frac{\Gamma}{2} \end{pmatrix}. \quad (\text{C25})$$

The characteristic polynomial of H_{exc} is

$$f(x) = x^2 - x(\delta - i\frac{\Gamma}{2}) - \frac{(\mu_{23}\mathcal{E})^2}{4}, \quad (\text{C26})$$

and EPs occur when the discriminant of the polynomial vanishes:

$$\Delta^2 \equiv (\frac{\delta}{2} - i\frac{\Gamma}{4})^2 + \frac{(\mu_{23}\mathcal{E})^2}{4} = 0 \quad (\text{C27})$$

Solving for \mathcal{E} and δ , we obtain the critical values⁶²:

$$\delta_{\text{EP}} = \frac{\Gamma \text{Im} \mu_{23}}{2 \text{Re} \mu_{23}} \quad \mathcal{E}_{\text{EP}} = \pm \frac{\Gamma}{2 \text{Re} \mu_{23}} \quad (\text{C28})$$

In the numerical calculation, we found EPs in the large ($MN \times MN$) Floquet Hamiltonian, including four field-free basis states and five Floquet bands, but found that the EP is obtained near the EP of the approximate 2×2 model. Specifically, we find an EP of the full Floquet Hamiltonian at $\delta \approx 1.001645 \delta_{\text{EP}}$ and $\mathcal{E} \approx 0.99420 \mathcal{E}_{\text{EP}}$.

IV. ELECTRONIC-STRUCTURE OF HELIUM

Table S1 summarizes the complex energies and transition dipole moments for lowest-energy single- and double-excitation states in helium. The numerical values were obtained by Kaprálová-Žďánská *et. al.*¹⁴, and are used in all the calculations in the main text. For comparison, we show additional ab-initio results from Ref. 68, which demonstrate good agreement between different methods for the set of energy levels that we consider.

TABLE S1. Complex energies (top) and transition dipole moments (bottom) for helium, obtained from ab-initio calculations in Refs. 14, 68.

		Re[E] ⁶⁸	Re[E] ¹⁴	Im[E] ⁶⁸	Im[E] ¹⁴
1	1s ²	-2.90372	-2.9035	0	0
2	1s2s	-2.14597	-2.1460	0	0
3	1s2p	-2.12384	-2.1238	0	0
4	2s ²	-0.777868	-0.7779	0.002271	-0.0023
5	2p ²	-0.710500	-0.7018	0.001181	-0.0012
6	2s2p	-0.693135	-0.6930	0.0006865	-0.0007
7	2p ²	-0.621926	-0.6216	0.000108	-0.0001

	μ_R ¹⁴	μ_I ¹⁴	λ [nm]
1 ↔ 3	0.4207	0.00000189	58.44 (UV)
1 ↔ 6	0.03599	0.01299	20.61 (UV)
2 ↔ 3	2.9167	0.000004652	2058.47 (IR)
2 ↔ 6	0.3130	-0.003598	31.36 (UV)
3 ↔ 4	-0.1231	-0.002554	33.85 (UV)
3 ↔ 5	0.3288	0.000193	32.04 (UV)
3 ↔ 7	-0.1925	0.0003475	30.33 (UV)
4 ↔ 6	1.5227	-0.00973	536.95 (visible)
5 ↔ 6	1.70545	-0.003767	5160.2 (IR)
6 ↔ 7	-2.1614	-0.001007	638.15 (visible)

¹F. Krausz and M. Ivanov, ‘‘Attosecond physics,’’ *Rev. Mod. Phys.* **81**, 163 (2009).

²J. Itatani, J. Levesque, D. Zeidler, H. Niikura, H. Pépin, J. C. Kieffer, P. B. Corkum, and D. M. Villeneuve, ‘‘Tomographic imaging of molecular orbitals,’’ *Nature* **432**, 867 (2004).

³P. M. Paul, E. S. Toma, P. Breger, G. Mullot, F. Augé, P. Balcou, H. G. Muller, and P. Agostini, ‘‘Observation of a train of attosecond pulses from high harmonic generation,’’ *Science* **292**, 1689–1692 (2001).

⁴K. Klünder, J. M. Dahlström, M. Gisselbrecht, T. Fordell, M. Swoboda, D. Guenot, P. Johnsson, J. Caillat, J. Mauritsson, A. Maquet, J. Caillat, J. Mauritsson, A. Maquet, and R. Taieb, ‘‘Probing single-photon ionization on the attosecond time scale,’’ *Phys. Rev. Lett.* **106**, 143002 (2011).

- ⁵D. Azoury, M. Krüger, G. Orenstein, H. R. Larsson, S. Bauch, B. D. Bruner, and N. Dudovich, “Self-probing spectroscopy of XUV photo-ionization dynamics in atoms subjected to a strong-field environment,” *Nature Comm.* **8**, 1453 (2017).
- ⁶H. Feshbach, “A unified theory of nuclear reactions. II,” *Ann. Phys.* **19**, 287–313 (1962).
- ⁷H. Friedrich and D. Wintgen, “Interfering resonances and bound states in the continuum,” *Phys. Rev. A* **32**, 3231 (1985).
- ⁸V. Averbukh and L. S. Cederbaum, “Ab-initio calculation of interatomic decay rates by a combination of the Fano ansatz, Green’s-function methods, and the stieljes imaging technique,” *J. Chem. Phys.* **123**, 204107 (2005).
- ⁹R. E. Goetz, T. A. Isaev, B. Nikoobakht, R. Berger, and C. P. Koch, “Theoretical description of circular dichroism in photoelectron angular distributions of randomly oriented chiral molecules after multi-photon photoionization,” *J. Chem. Phys.* **146**, 024306 (2017).
- ¹⁰N. Moiseyev, *Non-Hermitian Quantum Mechanics* (Cambridge University Press, 2011).
- ¹¹U. Fano, “Effects of configuration interaction on intensities and phase shifts,” *Phys. Rev.* **124**, 1866 (1961).
- ¹²S. H. Autler and C. H. Townes, “Stark effect in rapidly varying fields,” *Phys. Rev.* **100**, 703 (1955).
- ¹³T. Kato, *Perturbation Theory for Linear Operators*, Vol. 132 (Springer Science & Business Media, 2013).
- ¹⁴P. R. Kaprálová-Žďánská, J. Šmýdke, and S. Civiš, “Excitation of helium Rydberg states and doubly excited resonances in strong extreme ultraviolet fields: Full-dimensional quantum dynamics using exponentially tempered Gaussian basis sets,” *J. Chem. Phys.* **139**, 104314 (2013).
- ¹⁵P. R. Kaprálová-Žďánská and J. Šmýdke, “Gaussian basis sets for highly excited and resonance states of helium,” *J. Chem. Phys.* **138**, 024105 (2013).
- ¹⁶D. Zuev, T.-C. Jagau, K. B. Bravaya, E. Epifanovsky, Y. Shao, E. Sundstrom, M. Head-Gordon, and A. I. Krylov, “Complex absorbing potentials within eom-cc family of methods: Theory, implementation, and benchmarks,” *J. Chem. Phys.* **141**, 024102 (2014).
- ¹⁷A. Landau, I. Haritan, P. R. Kapralova-Zdanska, and N. Moiseyev, “Atomic and molecular complex resonances from real eigenvalues using standard (Hermitian) electronic structure calculations,” *J. Phys. Chem. A* **120**, 3098–3108 (2016).
- ¹⁸T. Fukuta, S. Garmon, K. Kanki, K.-I. Noba, and S. Tanaka, “Fano absorption spectrum with the complex spectral analysis,” *Phys. Rev. A* **96**, 052511 (2017).
- ¹⁹K. J. Boller, A. Imamoglu, and S. E. Harris, “Observation of electromagnetically induced transparency,” *Phys. Rev. Lett.* **66**, 2593 (1991).
- ²⁰S. E. Harris, J. E. Field, and A. Imamoglu, “Nonlinear optical processes using electromagnetically induced transparency,” *Phys. Rev. Lett.* **64**, 1107 (1990).
- ²¹S. E. Harris, “Electromagnetically induced transparency,” *Phys. Today* **50**, 36 (1997).
- ²²M. Fleischhauer and M. D. Lukin, “Dark-state polaritons in electromagnetically induced transparency,” *Phys. Rev. Lett.* **84**, 5094 (2000).
- ²³M. Fleischhauer, A. Imamoglu, and J. P. Marangos, “Electromagnetically induced transparency: Optics in coherent media,” *Rev. Mod. Phys.* **77**, 633 (2005).
- ²⁴A. Lezama, S. Barreiro, and A. M. Akulshin, “Electromagnetically induced absorption,” *Phys. Rev. A* **59**, 4732 (1999).
- ²⁵C. Goren, A. D. Wilson-Gordon, M. Rosenbluh, and H. Friedmann, “Electromagnetically induced absorption due to transfer of coherence and to transfer of population,” *Phys. Rev. A* **67**, 033807 (2003).
- ²⁶X. Zhang, N. Xu, K. Qu, Z. Tian, R. Singh, J. Han, G. S. Agarwal, and W. Zhang, “Electromagnetically induced absorption in a three-resonator metasurface system,” *Sci. Rep.* **5**, 10737 (2015).
- ²⁷N. E. Karapanagioti, O. Faucher, Y. L. Shao, D. Charalambidis, H. Bachau, and E. Cormier, “Observation of autoionization suppression through coherent population trapping,” *Phys. Rev. Lett.* **74**, 2431 (1995).
- ²⁸N. E. Karapanagioti, D. Charalambidis, C. J. G. J. Uiterwaal, C. Fotakis, H. Bachau, I. Sánchez, and E. Cormier, “Effects of coherent coupling of autoionizing states on multiphoton ionization,” *Phys. Rev. A* **53**, 2587 (1996).
- ²⁹T. Halfmann, L. P. Yatsenko, M. Shapiro, B. W. Shore, and K. Bergmann, “Population trapping and laser-induced continuum structure in helium: Experiment and theory,” *Phys. Rev. A* **58**, R46 (1998).
- ³⁰J. Y. Gao, S. H. Yang, D. Wang, X. Z. Guo, K. X. Chen, Y. Jiang, and B. Zhao, “Electromagnetically induced inhibition of two-photon absorption in sodium vapor,” *Phys. Rev. A* **61**, 023401 (2000).
- ³¹H. Bachau, P. Lambropoulos, and R. Shakeshaft, “Theory of laser-induced transitions between autoionizing states of He,” *Phys. Rev. A* **34**, 4785 (1986).
- ³²Y. J. Yan and S. Mukamel, “Eigenstate-free, Green function, calculation of molecular absorption and fluorescence line shapes,” *J. Chem. Phys.* **85**, 5908–5923 (1986).
- ³³M. W. Schmidt, K. K. Baldrige, J. A. Boatz, S. T. Elbert, M. S. Gordon, J. H. Jensen, S. Koseki, N. Matsunaga, K. A. Nguyen, S. Su, T. L. Windus, M. Dupuis, and J. A. Montgomery Jr, “General atomic and molecular electronic structure system,” *J. Comput. Chem.* **14**, 1347–1363 (1993).
- ³⁴S. Mukamel, *Principles of Nonlinear Optical Spectroscopy* (Oxford University Press on Demand, 1999).
- ³⁵L. N. Trefethen and D. Bau III, *Numerical Linear Algebra*, Vol. 50 (Siam, 1997).
- ³⁶G. B. Arfken and H. J. Weber, *Mathematical Methods for Physicists* (Elsevier Academic Press, 2006) pp. 184–185.
- ³⁷A. Shibatani and Y. Toyozawa, “Antiresonance in the optical absorption spectra of the impurity in solids,” *J. Phys. Soc. Jpn.* **25**, 335–345 (1968).
- ³⁸L. N. Trefethen and M. Embree, *Spectra and Pseudospectra: The Behavior of Nonnormal Matrices and Operators* (Princeton University Press, 2005).
- ³⁹D. J. Griffiths, *Introduction to Quantum Mechanics* (Upper Saddle River, NJ: Pearson Prentice Hall, 2005).
- ⁴⁰K. M. Lee, P. T. Leung, and K. M. Pang, “Dyadic formulation of morphology-dependent resonances. I. Completeness relation,” *JOSA B* **16**, 1409–1417 (1999).
- ⁴¹P. T. Leung, S. Y. Liu, and K. Young, “Completeness and orthogonality of quasinormal modes in leaky optical cavities,” *Phys. Rev. A* **49**, 3057 (1994).
- ⁴²G. W. Hanson, A. I. Nosich, and E. M. Kartchevski, “Green’s function expansions in dyadic root functions for shielded layered waveguides,” *PIER* **39**, 61–91 (2003).
- ⁴³E. Hernandez, A. Jauregui, and A. Mondragon, “Degeneracy of resonances in a double barrier potential,” *J. Phys. A* **33**, 4507–4523 (2000).
- ⁴⁴A. Hernández, E. Jauregui and A. Mondragon, “Jordan blocks and Gamow-Jordan eigenfunctions associated with a degeneracy of unbound states,” *Phys. Rev. A* **67**, 022721 (2003).
- ⁴⁵A. Pick, B. Zhen, O. D. Miller, C. W. Hsu, F. Hernandez, A. W. Rodriguez, M. Soljacic, and S. G. Johnson, “General theory of spontaneous emission near exceptional points,” *Opt. Exp.* **25**, 12325–12348 (2017).
- ⁴⁶Right and left eigenvectors satisfy the equations $\mathbb{H}\psi_i^R = \lambda_i \psi_i^R$ and $\mathbb{H}^T \psi_i^L = \lambda_i \psi_i^L$ respectively, where T denotes matrix transposition. When \mathbb{H} is Hermitian, one obtains $\mathbb{H}^* \psi_i^L = \lambda_i \psi_i^L$. Also, the eigenvalues of Hermitian operators are real. By complex-conjugating both sides of the last equation, one obtains $\mathbb{H}(\psi_i^L)^* = \lambda_i (\psi_i^L)^*$, which proves that $(\psi_i^L)^* \propto \psi_i^R$.
- ⁴⁷F. M. Penning, “Über ionisation durch metastabile atome,” *Naturwissenschaften* **15**, 818–818 (1927).
- ⁴⁸W. H. Miller, “Theory of Penning ionization. I. Atoms,” *J. Chem. Phys.* **52**, 3563–3572 (1970).
- ⁴⁹A. B. Henson, S. Gersten, Y. Shagam, J. Narevicius, and E. Narevicius, “Observation of resonances in Penning ionization reactions at sub-Kelvin temperatures in merged beams,” *Science* **338**, 234–238 (2012).
- ⁵⁰D. Bhattacharya, A. Ben-Asher, I. Haritan, M. Pawlak, A. Landau, and N. Moiseyev, “Polyatomic ab initio complex potential energy surfaces: Illustration of ultracold collisions,” *J. Chem. Theory Comput.* **13**, 1682–1690 (2017).
- ⁵¹L. S. Cederbaum, J. Zobeley, and F. Tarantelli, “Giant intermolecular decay and fragmentation of clusters,” *Phys. Rev. Lett.* **79**, 4778 (1997).
- ⁵²R. Santra, J. Zobeley, L. S. Cederbaum, and N. Moiseyev, “Interatomic Coulombic decay in van der Waals clusters and impact of nuclear motion,” *Phys. Rev. Lett.* **85**, 4490 (2000).
- ⁵³V. Averbukh, I. B. Müller, and L. S. Cederbaum, “Mechanism of interatomic Coulombic decay in clusters,” *Phys. Rev. Lett.* **93**, 263002 (2004).
- ⁵⁴S. T. Edwards, M. A. Johnson, and J. C. Tully, “Vibrational Fano resonances in dipole-bound anions,” *J. Chem. Phys.* **136**, 154305 (2012).
- ⁵⁵L. S. Cederbaum, “Ultrafast intermolecular energy transfer from vibrations to electronic motion,” *Phys. Rev. Lett.* **121**, 223001 (2018).
- ⁵⁶I. N. Levine, *Quantum Chemistry* (Upper Saddle River, N.J.: Prentice Hall, 2000).

- ⁵⁷T. Dittrich, P. Hänggi, G.-L. Ingold, B. Kramer, G. Schön, and W. Zwerger, “Quantum transport and dissipation,” (Wiley-Vch Weinheim, 1998) Chap. 5.
- ⁵⁸T. Bilitewski and N. R. Cooper, “Scattering theory for Floquet-Bloch states,” *Phys. Rev. A* **91**, 033601 (2015).
- ⁵⁹S. I. Chu and W. P. Reinhardt, “Intense field multiphoton ionization via complex dressed states: Application to the h atom,” *Phys. Rev. Lett.* **39**, 1195 (1977).
- ⁶⁰S. I. Chu, “Recent developments in semiclassical Floquet theories for intense-field multiphoton processes,” in *Adv. At. Mol. Phys.*, Vol. 21 (Elsevier, 1985) pp. 197–253.
- ⁶¹M. O. Scully and M. S. Zubairy, *Quantum Optics* (Cambridge University Press, 1997).
- ⁶²P. R. Kaprálová-Žďánská and N. Moiseyev, “Helium in chirped laser fields as a time-asymmetric atomic switch,” *J. Chem. Phys.* **141**, 014307 (2014).
- ⁶³A. A. Mailybaev, O. N. Kirillov, and A. P. Seyranian, “Geometric phase around exceptional points,” *Phys. Rev. A* **72**, 014104 (2005).
- ⁶⁴J. Doppler, A. A. Mailybaev, J. Bohm, U. Kuhl, A. Girschik, F. Libisch, T. J. Milburn, P. Rabl, N. Moiseyev, and S. Rotter, “Dynamically encircling an exceptional point for asymmetric mode switching,” *Nature* **537**, 76–79 (2016).
- ⁶⁵Z. Lin, A. Pick, M. Lončar, and A. W. Rodriguez, “Enhanced spontaneous emission at third-order dirac exceptional points in inverse-designed photonic crystals,” *Phys. Rev. Lett.* **117**, 107402 (2016).
- ⁶⁶E. Togan, Y. Chu, A. Imamoglu, and M. D. Lukin, “Laser cooling and real-time measurement of the nuclear spin environment of a solid-state qubit,” *Nature* **478**, 497 (2011).
- ⁶⁷A. P. Seyranian and A. A. Mailybaev, *Multiparameter Stability Theory With Mechanical Applications* (World Scientific Publishing, 2003).
- ⁶⁸I. Gilary, P. R. Kaprálová-Žďánská, and N. Moiseyev, “*Ab-initio* calculation of harmonic generation spectra of helium using a time-dependent non-hermitian formalism,” *Phys. Rev. A* **74**, 052505 (2006).